

Supporting Information for

“Covalency-Dependent Vibrational Dynamics in Two-Dimensional Titanium Carbides”

Tao Hu,^{†,*} Minmin Hu,^{†,‡} Zhaojin Li,^{†,‡} Hui Zhang,^{†,‡} Chao Zhang,[†] Jiemin Wang,[†] and Xiaohui Wang^{*,†}

[†]Shenyang National Laboratory for Materials Science, Institute of Metal Research, Chinese

Academy of Sciences, 72 Wenhua Road, Shenyang 110016, China

[‡]University of Chinese Academy of Sciences, Beijing 100049, China

Experiment and calculation details

***Ab initio* molecular dynamics**

To verify the structural stability of the system at elevated temperatures, we performed *ab initio* molecular dynamics calculations of the free-standing Ti_2CT_2 monosheet using the CASTEP code. We used the wave function extrapolation algorithm to cover time periods up to 0.5 ps with the time step of 1 fs. Results are presented in Fig. S1. At 273 K, the Ti_2CT_2 monosheet undergoes only minimal changes. Unless at a high temperature of 2000 K, significant structural changes can be found in $\text{Ti}_2\text{C}(\text{OH})_2$. The results indicate that the free-standing Ti_2CT_2 monosheet has robust stability and can maintain the free-standing structures at ambient temperature.

Preparation of Ti_2CT_2

The lamellae for the investigation were synthesized by exfoliating porous Ti_2AlC in hydrochloric acid (HCl) with NH_4HF_2 addition. Typically, porous Ti_2AlC (1.08 g) was immersed in a solution containing HCl (36.5%, 25 mL), NH_4HF_2 (1.50 g) and deionized water (15 mL). The porous Ti_2AlC was prepared by the method reported previously¹. The exfoliation process was carried out by immersing the porous Ti_2AlC monolith in the solution for 8 days at room temperature. After that,

the resulting sediment was washed several times using deionized water, followed by immersion in deionized water for one day and subsequent vacuum filtration. The collected powder was dried by cryodesiccation.

XRD and SEM

The as-synthesized Ti_2CT_2 samples were examined by XRD (Rigaku D/max-2400, Tokyo, Japan) with $\text{Cu K}\alpha$ radiation ($\lambda = 1.54178 \text{ \AA}$) at a scanning speed of 0.04 step^{-1} . Morphological studies of the prepared lamella were conducted by SEM (LEO Supra 35, Germany).

Raman spectroscopy

As an efficient and non-destructive method for surface analysis, nanostructure investigation and vibration analysis, Raman spectroscopy is very sensitive to tiny changes in crystal structure. To gain insight into the structure, we also carried out Raman measurements of experimentally achieved lamellae. The unpolarized Raman spectra of the exfoliated lamellae were collected on a LabRAM HR800 (Jobin Yvon, France) equipped with an air-cooled CCD array detector in the backscattering configuration. For the Raman measurements, a long-working-distance 50 \times objective with numerical aperture of 0.50 was used. A He–Ne laser ($\lambda = 632.8 \text{ nm}$) was used and the laser power was kept below 4 mW on the sample surface to avoid laser-induced heating. A grating of 1800 lines/mm was used for single Raman spectrum measurement to achieve high spectral resolution. The temperature-dependent Raman measurements were carried out on a THMS 600 temperature-controlled stage (Linkam, England). Liquid nitrogen was used as a cooling agent, which was pumped into the stage by a liquid nitrogen cooling pump. The sample temperature was controlled by a programmable THMS 600 temperature-controlled stage with the accuracy of 0.1 K. The sample was cooled to desired temperature and held for 10 minutes before recording Raman spectrum. The testing temperature ranges from $-190 \text{ }^\circ\text{C}$ to $10 \text{ }^\circ\text{C}$ with a step of $50 \text{ }^\circ\text{C}$.

Tables

Table S1. Calculated lattice constants of Ti_2AlC and Ti_3AlC_2 with present calculation scheme and data available from previous works

	Lattice constants	a (Å)	c (Å)
Ti_2AlC	Calculated	3.06	13.76
	Available data	$3.06^2, 3.04^3$	$13.67^2, 13.60^3$
Ti_3AlC_2	Calculated	3.08	18.67
	Available data	$3.07^4, 3.08^{5,6}$	$18.58^4, 18.64^5, 18.65^6$

Table S2. Calculated wavenumbers (in cm^{-1}) of Raman active modes of Ti_2AlC and Ti_3AlC_2 with present calculation scheme and data available from previous works

	Modes	ω_1 (E_{2g})	ω_2 (E_{1g})	ω_3 (E_{2g})	ω_4 (E_{1g})	ω_5 (E_{1g} and E_{2g})	ω_6 (A_{1g})
Ti_2AlC	Calculated	148	263	266	360		
	Experimental ⁷		270	270	364		
	Experimental ⁸	150	262	268	365		
Ti_3AlC_2	Calculated	126	181	197	268	615 and 617	657
	Calculated ⁹	125	182	197	268	620 and 621	655
	Experimental ⁷		182		270		658
	Experimental ⁹		183	201	270	632	663

Table S3. Cophonicity metric. Cophonicity (C_{ph} , in cm^{-1}) of adjacent atomic pair of Ti_2CT_2 and $\text{Ti}_3\text{C}_2\text{T}_2$ with the same calculation scheme. The smaller is $C_{\text{ph, A-B}}$, the higher is the mixing of the A and B contributions to the frequency band, and the two atoms have the same weight in the determination of the modes specific of the considered energy range¹⁰. The frequency range used to calculate the cophonicity metric is over all the frequencies in the phonon dispersion curve.

	$C_{\text{ph, Ti-C}}$	$C_{\text{ph, Ti-T}}$	$C_{\text{ph, O-H}}$		$C_{\text{ph, Ti1-C}}$	$C_{\text{ph, Ti2-C}}$	$C_{\text{ph, Ti2-T}}$	$C_{\text{ph, O-H}}$
Ti_2C	326.97			Ti_3C_2	284.71	319.80		
Ti_2CO_2	311.29	178.92		$\text{Ti}_3\text{C}_2\text{O}_2$	269.73	301.89	169.59	
Ti_2CF_2	348.70	1.01		$\text{Ti}_3\text{C}_2\text{F}_2$	296.15	318.92	11.69	
$\text{Ti}_2\text{C}(\text{OH})_2$	337.93	132.23(Ti-O)	1089.60	$\text{Ti}_3\text{C}_2(\text{OH})_2$	304.48	319.74	124.90(Ti-O)	1101.80

Table S4. Speed of sound calculated by the slope of longitudinal acoustic branches near Γ in phonon dispersions of Ti_2C and Ti_2CT_2 ($T = \text{O, F, OH}$) monosheets. The results indicate that the in-plane elastic response of four MXenes is nearly isotropic

	$v_s^{\Gamma-\text{M}}$ (km/s)	$v_s^{\Gamma-\text{K}}$ (km/s)
Ti_2C	7.065	7.096
Ti_2CO_2	9.263	9.376
Ti_2CF_2	7.605	7.611
Ti_2COH_2	7.442	7.448

Table S5. Assignment of Raman active vibration modes of Ti_2C and Ti_2CT_2 ($T = \text{O}, \text{F}, \text{OH}$)

monosheets

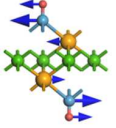
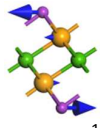
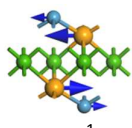
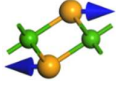
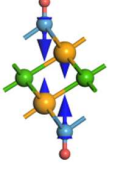
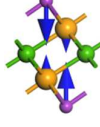
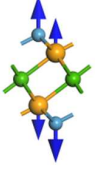
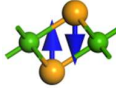
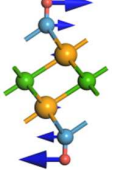
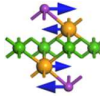
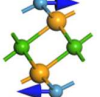
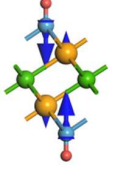
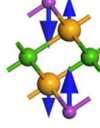
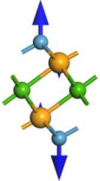
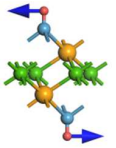
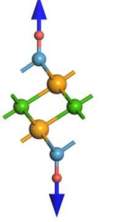
Formula	$\text{Ti}_2\text{C}(\text{OH})_2$	Ti_2CF_2	Ti_2CO_2	Ti_2C
Modes				
$\omega_1 (E_g)$	 192 cm^{-1}	 192 cm^{-1}	 128 cm^{-1}	 236 cm^{-1}
$\omega_2 (A_{1g})$	 288 cm^{-1}	 283 cm^{-1}	 293 cm^{-1}	 333 cm^{-1}
$\omega_3 (E_g)$	 283 cm^{-1}	 254 cm^{-1}	 409 cm^{-1}	
$\omega_4 (A_{1g})$	 528 cm^{-1}	 505 cm^{-1}	 596 cm^{-1}	
$\omega_5 (E_g)$	 445 cm^{-1}			
$\omega_6 (A_{1g})$	 3707 cm^{-1}			

Table S6. Assignment of IR active vibration modes of Ti_2C and Ti_2CT_2 ($T = \text{O}, \text{F}, \text{OH}$) monosheets

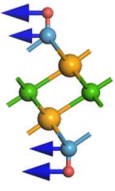
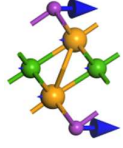
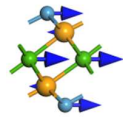
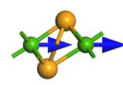
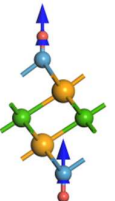
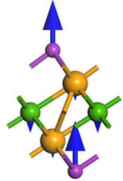
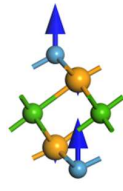
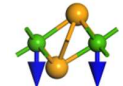
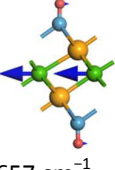
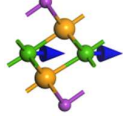
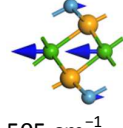
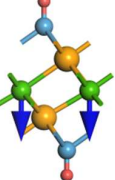
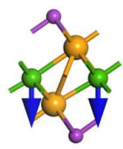
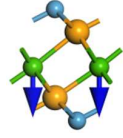
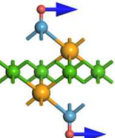
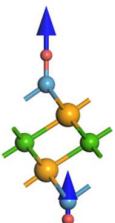
Formula	$\text{Ti}_2\text{C}(\text{OH})_2$	Ti_2CF_2	Ti_2CO_2	Ti_2C
Modes				
$\omega_1 (E_u)$	 286 cm^{-1}	 257 cm^{-1}	 240 cm^{-1}	 637 cm^{-1}
$\omega_2 (A_{2u})$	 489 cm^{-1}	 451 cm^{-1}	 578 cm^{-1}	 520 cm^{-1}
$\omega_3 (E_u)$	 657 cm^{-1}	 669 cm^{-1}	 505 cm^{-1}	
$\omega_4 (A_{2u})$	 633 cm^{-1}	 666 cm^{-1}	 741 cm^{-1}	
$\omega_5 (E_u)$	 444 cm^{-1}			
$\omega_6 (A_{2u})$	 3701 cm^{-1}			

Table S7. Covalency metric. Bond Covalency (in eV) of adjacent atomic pair of Ti_2CT_2 and $\text{Ti}_3\text{C}_2\text{T}_2$ with same calculation scheme. The greater the value of $C_{\text{A-B}}$, the higher the overlap of the selected atomic bands, and thus the electron density described by those orbitals gives a more covalent A–B bond. The quantity $C_{\text{A-B}}$ is denoted as the covalency of the A–B bond, which is specified in units of $\text{eV}^{10,11}$. The energy range used to calculate the covalency metric is over all the energies in the electronic band structure, specifically, $[-60, 15]$ eV.

	$C_{\text{Ti-C}}$	$C_{\text{Ti-T}}$	$C_{\text{O-H}}$		$C_{\text{Ti1-C}}$	$C_{\text{Ti2-C}}$	$C_{\text{Ti2-T}}$	$C_{\text{O-H}}$
Ti_2C	–10.72			Ti_3C_2	–13.14	–11.53		
Ti_2CO_2	–12.33	–7.75		$\text{Ti}_3\text{C}_2\text{O}_2$	–13.89	–13.82	–10.34	
Ti_2CF_2	–11.23	–3.72		$\text{Ti}_3\text{C}_2\text{F}_2$	–13.66	–12.84	–6.16	
$\text{Ti}_2\text{C}(\text{OH})_2$	–12.27	–6.78(Ti–O)	–4.67	$\text{Ti}_3\text{C}_2(\text{OH})_2$	–13.24	–12.92	–7.94(Ti2–O)	–3.31

Figures

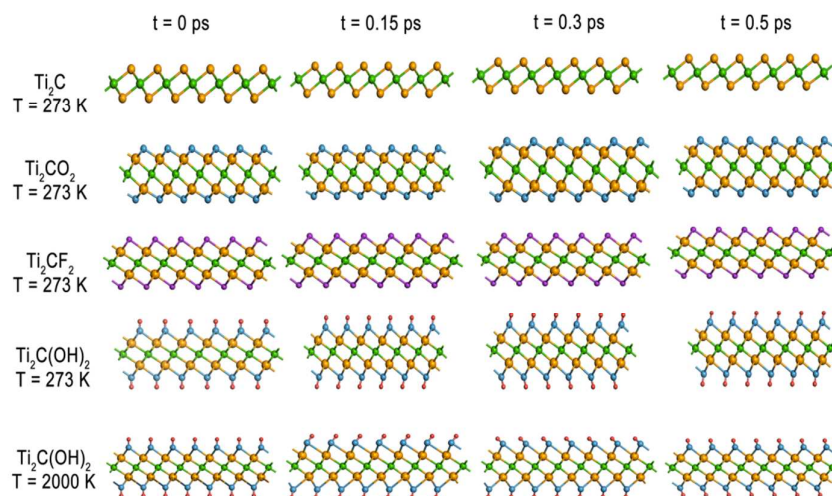


Figure S1. Snap shots of canonical molecular dynamics simulations depicting structural changes in a free-standing Ti_2CT_2 monosheet at different temperatures. A $6 \times 6 \times 1$ supercell was used.

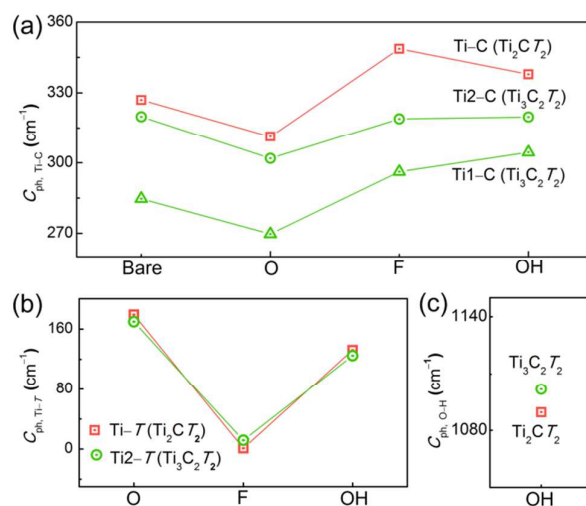


Figure S2. Cophonicity of Ti_2CT_2 and $\text{Ti}_3\text{C}_2\text{T}_2$ monosheet. (a) Ti-C, (b) Ti-T and (c) O-H.

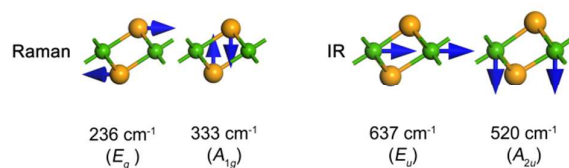


Figure S3. Schematics of Raman and infrared active vibration modes of Ti_2C monosheet.

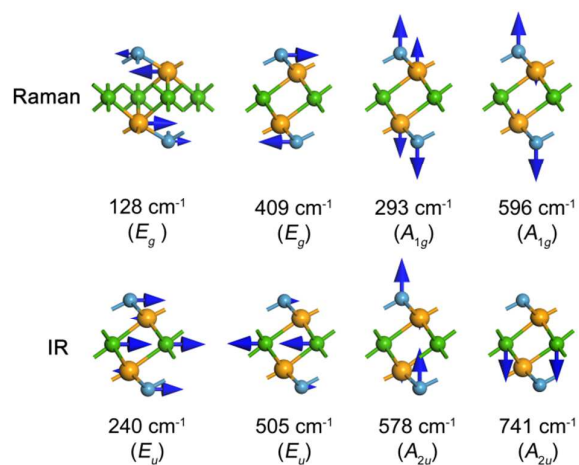


Figure S4. Schematics of Raman and infrared active vibration modes of Ti_2CO_2 monosheet.

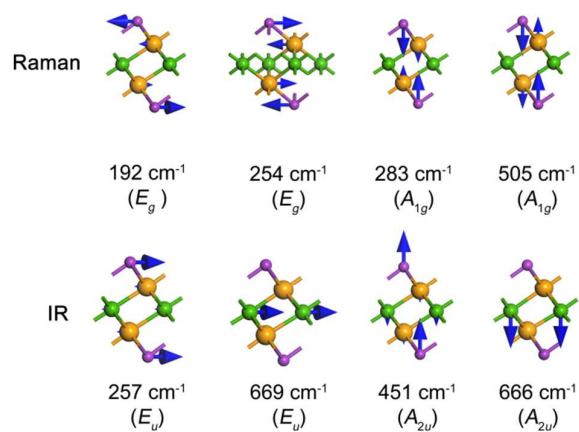


Figure S5. Schematics of Raman and infrared active vibration modes of Ti_2CF_2 monosheet.

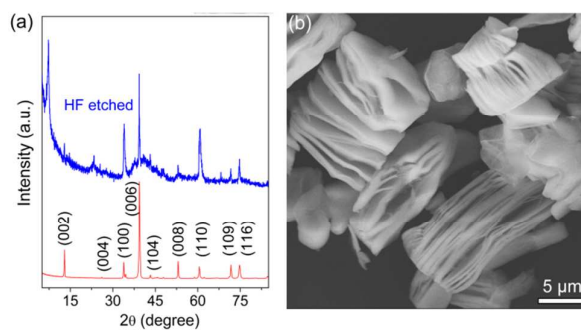


Figure S6. (a) XRD pattern for Ti_2AlC before and after HF treatment; (b) SEM image of experimentally obtained lamellae. (b) shows a 2000 \times magnitude image of the lamellae.

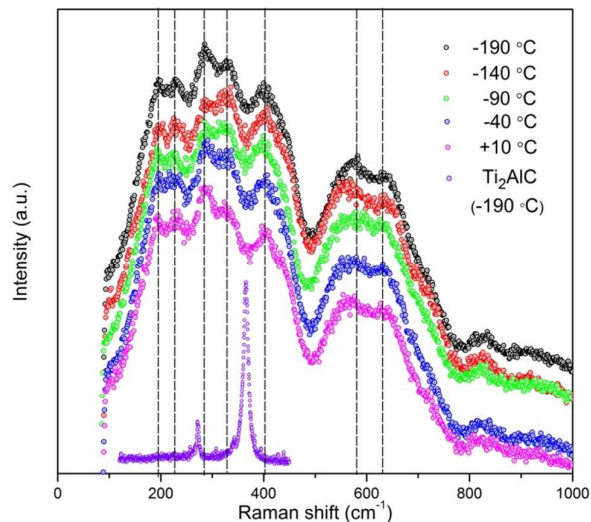


Figure S7. Micro Raman spectra of exfoliated Ti_2CT_2 lamellae at various temperatures. For the sake of comparison, Raman spectrum of Ti_2AlC at -190°C is also included. Note that all the Raman peaks of Ti_2AlC are well below 500 cm^{-1} from both theoretical (See Table S2) and experimental aspects, while the exfoliated Ti_2CT_2 lamellae possess several obvious bands above 500 cm^{-1} .

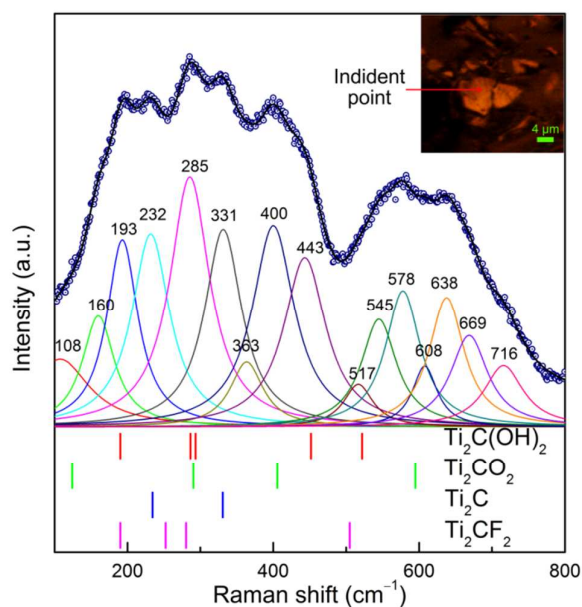


Figure S8. Micro Raman spectrum of experimentally obtained lamellae. Calculated Raman active frequencies of Ti_2C and Ti_2CT_2 monosheets are also included. Inset shows image of lamellae. The bands at 638 , 669 and 716 cm^{-1} probably stems from the changes in symmetry with increasing Ti_2CT_2 layers, which makes IR active modes $633\text{ (A}_{2u})$, $666\text{ (A}_{2u})$ and $741\text{ (A}_{2u})\text{ cm}^{-1}$ change to Raman active modes, as in MoS_2 .¹²

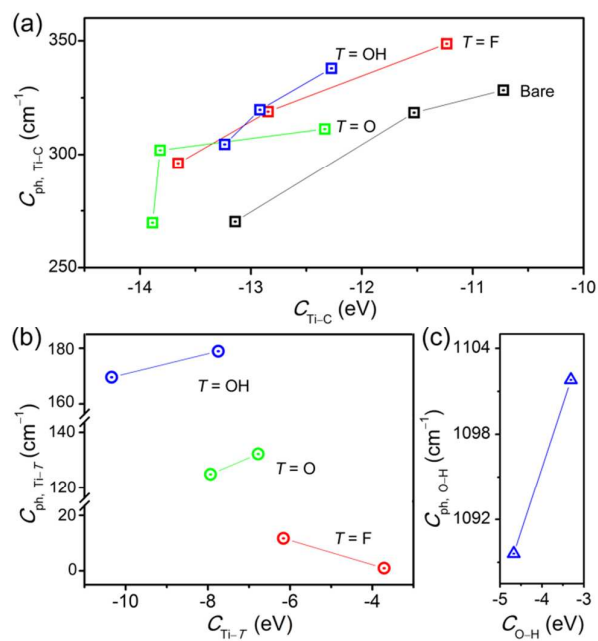


Figure S9. Correlation between covalency and cophonicity of (a) Ti-C, (b) Ti-T and (c) O-H atomic pair. The plot generally shows a positive correlation between covalency and cophonicity in the studied system except the Ti-F atomic pair in $\text{Ti}_{n+1}\text{C}_n\text{F}_2$ monosheet.

- (1) Wang, X. H.; Zhou, Y. C. Solid-Liquid Reaction Synthesis and Simultaneous Densification of Polycrystalline Ti_2AlC . *Z. Metallkd.* **2002**, *93*, 66–71.
- (2) Sun, Z. M.; Ahuja, R.; Li, S.; Schneider, J. M. Structure and Bulk Modulus of $M_2\text{AlC}$ ($M = \text{Ti, V, and Cr}$). *Appl. Phys. Lett.* **2003**, *83*, 899.
- (3) Schuster, J. C.; Nowotny, H.; Vaccaro, C. The Ternary-Systems: Cr-Al-C, V-Al-C, and Ti-Al-C and the Behavior of H-Phases ($M_2\text{AlC}$). *J. Solid State Chem.* **1980**, *32*, 213–219.
- (4) Wang, X. H.; Zhou, Y. C. Layered Machinable and Electrically Conductive Ti_2AlC and Ti_3AlC_2 Ceramics: A Review. *J. Mater. Sci. Tech.* **2010**, *26*, 385–416.
- (5) Xie, Y.; Kent, P. R. C. Hybrid Density Functional Study of Structural and Electronic Properties of Functionalized $\text{Ti}_{n+1}\text{X}_n$ ($X = \text{C, N}$) Monolayers. *Phys. Rev. B* **2013**, *87*, 235441.
- (6) Shein, I. R.; Ivanovskii, A. L. Graphene-Like Titanium Carbides and Nitrides $\text{Ti}_{n+1}\text{C}_n$, $\text{Ti}_{n+1}\text{N}_n$ ($n = 1, 2$, and 3) from De-Intercalated MAX Phases: First-Principles Probing of Their Structural, Electronic Properties and Relative Stability. *Computational Materials Science* **2012**, *65*, 104–114.
- (7) Zhang, H.; Wang, X. H.; Xiang, H. M.; Li, Z. J.; Zhou, Y. C. Micro-Raman Spectroscopic Study of Nanolaminated $\text{Ti}_5\text{Al}_2\text{C}_3$. *Appl. Phys. Lett.* **2014**, *104*, 131903.
- (8) Spanier, J. E.; Gupta, S.; Amer, M.; Barsoum, M. W. Vibrational Behavior of The $M_{n+1}\text{AX}_n$ phases from First-Order Raman Scattering ($M = \text{Ti, V, Cr, A = Si, X = C, N}$). *Phys. Rev. B* **2005**, *71*, 012103.
- (9) Presser, V.; Naguib, M.; Chaput, L.; Togo, A.; Hug, G.; Barsoum, M. W. First-Order Raman Scattering of the MAX Phases: Ti_2AlN , $\text{Ti}_2\text{AlC}_{0.5}\text{N}_{0.5}$, Ti_2AlC , $(\text{Ti}_{0.5}\text{V}_{0.5})_2\text{AlC}$, V_2AlC , Ti_3AlC_2 , and Ti_3GeC_2 . *J. Raman Spectrosc.* **2012**, *43*, 168–172.
- (10) Cammarata, A.; Polcar, T. Tailoring Nanoscale Friction in MX_2 Transition Metal Dichalcogenides. *Inorg. Chem.* **2015**, *54*, 5739–5744.
- (11) Cammarata, A.; Rondinelli, J. M. Covalent Dependence of Octahedral Rotations in Orthorhombic Perovskite Oxides. *J. Chem. Phys.* **2014**, *141*, 114704.
- (12) Staiger, M.; Gillen, R.; Scheuschner, N.; Ochedowski, O.; Kampmann, F.; Schleberger, M.; Thomsen, C.; Maultzsch, J. Splitting of Monolayer out-of-Plane A_1' Raman Mode in Few-Layer WS_2 . *Phys. Rev. B* **2015**, *91*, 195419.